Figure Legends

Figure1: Notch signaling is decreased in human Barrett's esophagus. (A) Microarray analysis from seven Barrett's esophagus and seven paired normal squamous esophagus for status of Notch signaling pathway, GEO accession # (GSE 13083). (B) Representative image of normal esophagus and Barrett's esophagus tissue from tissue microarray (TMA) stained for NOTCH1, ICN1 and HES1 (200X Magnification). (C) Average scoring for positive staining in the TMA and statistical analysis Fisher's exact t-test.

Figure 2: Inhibition of Notch signaling in esophageal epithelial cells changes basal cell morphology in 3D cultures. (A) Western blotting for GFP (dnMAML), MYC and CDX1 in EPC2-hTERT, MYC-CDX1 and MYC-CDX1-dnMAML cells. (B) Luciferase assay with Notch-responsive pGL3-8XCSL reporter vector in MYC-CDX1-ICN1 and MYC-CDX1-ICN1-dnMAML cells, graph represents mean ± SEM (n=3). Student t-test was performed to determine significance, *p≤0.05. (C) Quantitative PCR (qPCR) for Notch downstream targets HES1 and HES5 in MYC-CDX1 and MYC-CDX1-dnMAML cells. Graph represents mean ± SEM (n=3) and student t-test was performed to determine significance, ≤*p 0.05. (D) H&E staining of representative 3D organotypic cultures of MYC-CDX1 and MYC-CDX1-dnMAML cells, arrow indicates elongated cells,(Magnification 200X). (E) Electron microscopy of MYC-CDX1 and MYC-CDX1-dnMAML 3D organotypic cultures, scale bars=0.2μm. (F) Graph represents relative height of MYC-CDX1 and MYC-CDX1-dnMAML basal layer cells mean ± SEM (n=4). Student t-test was performed to determine significance, *p<0.0001.

Figure 3: Inhibition of Notch signaling in esophageal epithelial cells decreases squamous K13+ cells and increases columnar K19+ cells in 3D organotypic culture. IHC staining of 3D organotypic cultures for squamous keratin K13 (A) and columnar keratin K19 (B) in MYC-CDX1 (left panel) and MYC-CDX1-dnMAML cultures (right panel) (200X and 400X Magnification).

Figure 4: Inhibition of Notch signaling in esophageal epithelial cells promotes a switch from the squamous lineage to a columnar lineage. (A) qPCR of squamous keratins K5, K13 and K14; (B) of columnar keratins K8, K18, K19 and K20; (C) of mucin genes MUC2, MUC3B, MUC5B and MUC17; (D) and of differentiation genes DSC1, and DSC3 in MYC-CDX1 and MYC-CDX1-dnMAML cells. Graph represents mean ± SEM (n=6). Student t-test was performed to determine significance, *p≤0.05, **p≤0.001.

Figure 5: Knockdown of KLF4 expression reverses partially the morphological changes induced by Notch signaling inhibition in 3D cultures. (A) qPCR of KLF4 expression in MYC-CDX1 and MYC-CDX1-dnMAML cells. (B) Western blotting for KLF4 in EPC2-hTERT, MYC-CDX1 and MYC-CDX1-dnMAML cells. (C) qPCR of KLF4 in MYC-CDX1-dnMAML-shScramble and MYC-CDX1-dnMAML-shKLF4 cells. (D) Western blotting for KLF4 in MYC-CDX1-dnMAML-shScramble and MYC-CDX1-dnMAML-shKLF4 cells. (E) H&E staining of MYC-CDX1-dnMAML-shScramble and MYC-CDX1-dnMAML-shKLF4 3D organotypic cultures (400X Magnification). Graph represents mean ± SEM (n=6). Student t-test was performed to determine significance, *p≤0.01.

Figure 6: Knockdown of KLF4 reverses lineage changes induced by Notch signaling in esophageal keratinocytes. (A) qPCR of columnar keratins K8, K18, K19 and K20; (B) of mucin genes MUC2, MUC3B, MUC5B and MUC17; (C) of squamous keratins K5, K13 and K14; (D) and of squamous differentiation markers DSC1 and DSC3 in MYC-CDX1-dnMAML-shScramble and MYC-CDX1-dnMAML-shKLF4 cells. Graph represents mean ± SEM (n=6). Student t-test was performed to determine significance, *p≤0.01, **p≤0.001.

Figure 7: Model. Inhibition of Notch signaling in conjunction with MYC and CDX1 expression promotes increased expression of columnar keratins and mucin genes as well as decreased expression of squamous keratins and other markers of differentiation. Inhibition of Notch also triggers changes in cell morphology in the basal layer. Inhibition of Notch signaling promotes KLF4 expression and the initiation of a transdifferentiation program towards a BE-like metaplasia.

References

1. Fitzgerald RC. Molecular basis of Barrett's oesophagus and oesophageal adenocarcinoma. Gut 2006;55:1810-1820.

2. Hayeck TJ, Kong CY, Spechler SJ, Gazelle GS, Hur C. The prevalence of Barrett's esophagus in the US: estimates from a simulation model confirmed by SEER data. Dis Esophagus 2010;23:451-457.

3. Reid BJ, Li X, Galipeau PC, Vaughan TL. Barrett's oesophagus and oesophageal adenocarcinoma: time for a new synthesis. Nat Rev Cancer 2010;10:87-101.

4. Howlader N, Noone A, Krapcho M, et al. SEER Cancer Statistics Factsheets: Esophageal Cancer. National Cancer Institute. Bethesda, MD; April, 2013. Available at: http://seer.cancer.gov/statfacts/html/esoph.html. Accessed March, 27, 2014.

5. Graham TA, McDonald SA. Genetic diversity during the development of Barrett's oesophagus-associated adenocarcinoma: how, when and why? Biochem Soc Trans 2010;38:374-379.

6. DeVault K, McMahon BP, Celebi A, et al. Defining esophageal landmarks, gastroesophageal reflux disease, and Barrett's esophagus. Ann N Y Acad Sci 2013;1300:278-295.

7. Quante M, Abrams JA, Lee Y, Wang TC. Barrett esophagus: what a mouse model can teach us about human disease. Cell Cycle 2012;11:4328-4338.

8. Quante M, Bhagat G, Abrams JA, et al. Bile acid and inflammation activate gastric cardia stem cells in a mouse model of Barrett-like metaplasia. Cancer Cell 2012;21:36-51.

9. Sarosi G, Brown G, Jaiswal K, et al. Bone marrow progenitor cells contribute to esophageal regeneration and metaplasia in a rat model of Barrett's esophagus. Dis Esophagus 2008;21:43-50.

10. Stairs DB, Nakagawa H, Klein-Szanto A, et al. Cdx1 and c-Myc foster the initiation of transdifferentiation of the normal esophageal squamous epithelium toward Barrett's esophagus. PLoS One 2008;3:e3534.

11. Guo RJ, Suh ER, Lynch JP. The role of Cdx proteins in intestinal development and cancer. Cancer Biol Ther 2004;3:593-601.

12. Gao N, White P, Kaestner KH. Establishment of intestinal identity and epithelial-mesenchymal signaling by Cdx2. Dev Cell 2009;16:588-599.

13. Herold S, Herkert B, Eilers M. Facilitating replication under stress: an oncogenic function of MYC? Nat Rev Cancer 2009;9:441-444.

14. Meyer N, Penn LZ. Reflecting on 25 years with MYC. Nat Rev Cancer 2008;8:976-990.

15. Ruggero D. The role of Myc-induced protein synthesis in cancer. Cancer Res 2009;69:8839-8843.

16. von Rahden BH, Stein HJ, Puhringer-Oppermann F, Sarbia M. c-myc amplification is frequent in esophageal adenocarcinoma and correlated with the upregulation of VEGF-A expression. Neoplasia 2006;8:702-707.

17. Harada H, Nakagawa H, Oyama K, et al. Telomerase induces immortalization of human esophageal keratinocytes without p16INK4a inactivation. Mol Cancer Res 2003;1:729-738.

18. Harada H, Nakagawa H, Oyama K, et al. Telomerase induces immortalization of human esophageal keratinocytes without p16INK4a inactivation. Mol Cancer Res 2003;1:729-738.

19. van Es JH, van Gijn ME, Riccio O, et al. Notch/gamma-secretase inhibition turns proliferative cells in intestinal crypts and adenomas into goblet cells. Nature 2005;435:959-963.

20. Fre S, Huyghe M, Mourikis P, Robine S, Louvard D, Artavanis-Tsakonas S. Notch signals control the fate of immature progenitor cells in the intestine. Nature 2005;435:964-968.

21. Zecchini V, Domaschenz R, Winton D, Jones P. Notch signaling regulates the differentiation of post-mitotic intestinal epithelial cells. Genes Dev 2005;19:1686-1691.

22. Menke V, van Es JH, de Lau W, et al. Conversion of metaplastic Barrett's epithelium into post-mitotic goblet cells by gamma-secretase inhibition. Dis Model Mech 2010;3:104-110.

23. LaVoie MJ, Selkoe DJ. The Notch ligands, Jagged and Delta, are sequentially processed by alpha-secretase and presenilin/gamma-secretase and release signaling fragments. J Biol Chem 2003;278:34427-34437.

24. Benedito R, Roca C, Sorensen I, et al. The notch ligands Dll4 and Jagged1 have opposing effects on angiogenesis. Cell 2009;137:1124-1135.

25. Weinmaster G. The ins and outs of notch signaling. Mol Cell Neurosci 1997;9:91-102.

26. Zheng H, Pritchard DM, Yang X, et al. KLF4 gene expression is inhibited by the notch signaling pathway that controls goblet cell differentiation in mouse gastrointestinal tract. Am J Physiol Gastrointest Liver Physiol 2009;296:G490-8.

27. Ghaleb AM, Aggarwal G, Bialkowska AB, Nandan MO, Yang VW. Notch inhibits expression of the Kruppel-like factor 4 tumor suppressor in the intestinal epithelium. Mol Cancer Res 2008;6:1920-1927.

28. McConnell BB, Yang VW. Mammalian Kruppel-like factors in health and diseases. Physiol Rev 2010;90:1337-1381.

29. Kazumori H, Ishihara S, Takahashi Y, Amano Y, Kinoshita Y. Roles of Kruppel-like factor 4 in oesophageal epithelial cells in Barrett's epithelium development. Gut 2011;60:608-617.

30. Grugan KD, Miller CG, Yao Y, et al. Fibroblast-secreted hepatocyte growth factor plays a functional role in esophageal squamous cell carcinoma invasion. Proc Natl Acad Sci U S A 2010;107:11026-11031.

31. Kalabis J, Wong GS, Vega ME, et al. Isolation and characterization of mouse and human esophageal epithelial cells in 3D organotypic culture. Nat Protoc 2012;7:235-246.

32. Ohashi S, Natsuizaka M, Wong GS, et al. Epidermal growth factor receptor and mutant p53 expand an esophageal cellular subpopulation capable of epithelial-to-mesenchymal transition through ZEB transcription factors. Cancer Res 2010;70:4174-4184.

33. Zheng JL, Shou J, Guillemot F, Kageyama R, Gao WQ. Hes1 is a negative regulator of inner ear hair cell differentiation. Development 2000;127:4551-4560.

34. Kazanjian A, Noah T, Brown D, Burkart J, Shroyer NF. Atonal homolog 1 is required for growth and differentiation effects of notch/gamma-secretase inhibitors on normal and cancerous intestinal epithelial cells. Gastroenterology 2010;139:918-28, 928.e1-6.

35. Hahn HP, Blount PL, Ayub K, et al. Intestinal differentiation in metaplastic, nongoblet columnar epithelium in the esophagus. Am J Surg Pathol 2009;33:1006-1015.

36. Ohashi S, Natsuizaka M, Yashiro-Ohtani Y, et al. NOTCH1 and NOTCH3 coordinate esophageal squamous differentiation through a CSL-dependent transcriptional network. Gastroenterology 2010;139:2113-2123.

37. Tamagawa Y, Ishimura N, Uno G, et al. Notch signaling pathway and Cdx2 expression in the development of Barrett's esophagus. Lab Invest 2012;92:896-909.

38. Yoshida T, Yamashita M, Hayashi M. Kruppel-like factor 4 contributes to high phosphate-induced phenotypic switching of vascular smooth muscle cells into osteogenic cells. J Biol Chem 2012;287:25706-25714.

39. Kim J, Efe JA, Zhu S, et al. Direct reprogramming of mouse fibroblasts to neural progenitors. Proc Natl Acad Sci U S A 2011;108:7838-7843.

40. Efe JA, Hilcove S, Kim J, et al. Conversion of mouse fibroblasts into cardiomyocytes using a direct reprogramming strategy. Nat Cell Biol 2011;13:215-222.

41. Fang Y, Chen X, Bajpai M, et al. Cellular origins and molecular mechanisms of Barrett's esophagus and esophageal adenocarcinoma. Ann N Y Acad Sci 2013;1300:187-199.

42. Clement G, Guilleret I, He B, et al. Epigenetic alteration of the Wnt inhibitory factor-1 promoter occurs early in the carcinogenesis of Barrett's esophagus. Cancer Sci 2008;99:46-53.

43. Yang L, Wang LS, Chen XL, et al. Hedgehog signaling activation in the development of squamous cell carcinoma and adenocarcinoma of esophagus. Int J Biochem Mol Biol 2012;3:46-57.

44. Okawa T, Michaylira CZ, Kalabis J, et al. The functional interplay between EGFR overexpression, hTERT activation, and p53 mutation in esophageal epithelial cells with activation of stromal fibroblasts induces tumor development, invasion, and differentiation. Genes Dev 2007;21:2788-2803.

45. Pear WS, Scott ML, Nolan GP. Generation of high-titer, helper-free retroviruses by transient transfection. Methods Mol Med 1997;7:41-57.

46. Moffat J, Grueneberg DA, Yang X, et al. A lentiviral RNAi library for human and mouse genes applied to an arrayed viral high-content screen. Cell 2006;124:1283-1298.

47. Grugan KD, Vega ME, Wong GS, et al. A common p53 mutation (R175H) activates c-Met receptor tyrosine kinase to enhance tumor cell invasion. Cancer Biol Ther 2013;14:.

FIGURE 1

A

Gene Symbol	Fold (BE vs. norm.)	p-value (BE vs. norm.)
NOTCH2	-4.41726	4.62E-06
NOTCH2	-4.80363	7.95E-07
NOTCH3	-6.3073	2.94E-03
JAG1	-2.66073	1.02E-04
JAG1	-2.80861	1.50E-04
JAG1	-3.72515	7.20E-04

C

Staining/IHC	Average Score		p-value
	Normal Esophagus	Barrett's Esophagus (BE)	BE vs norm.
NOTCH1	1.8	0.5	<0.0001
ICN1	0.8	0.14	0.00017
HES1	1.1	0.4	0.018

B

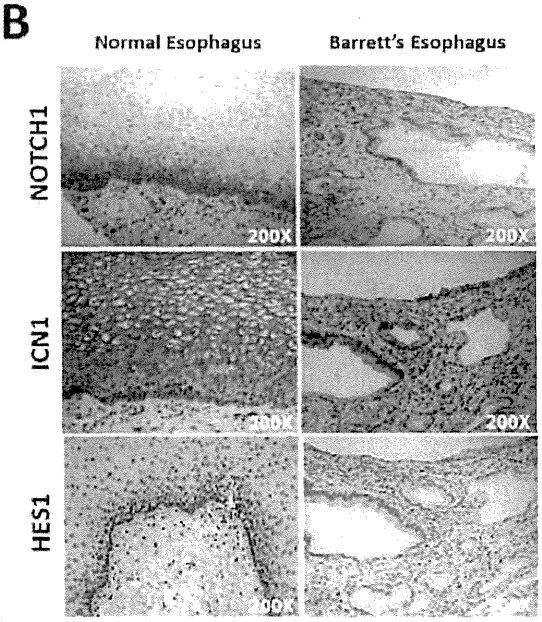

FIGURE 2

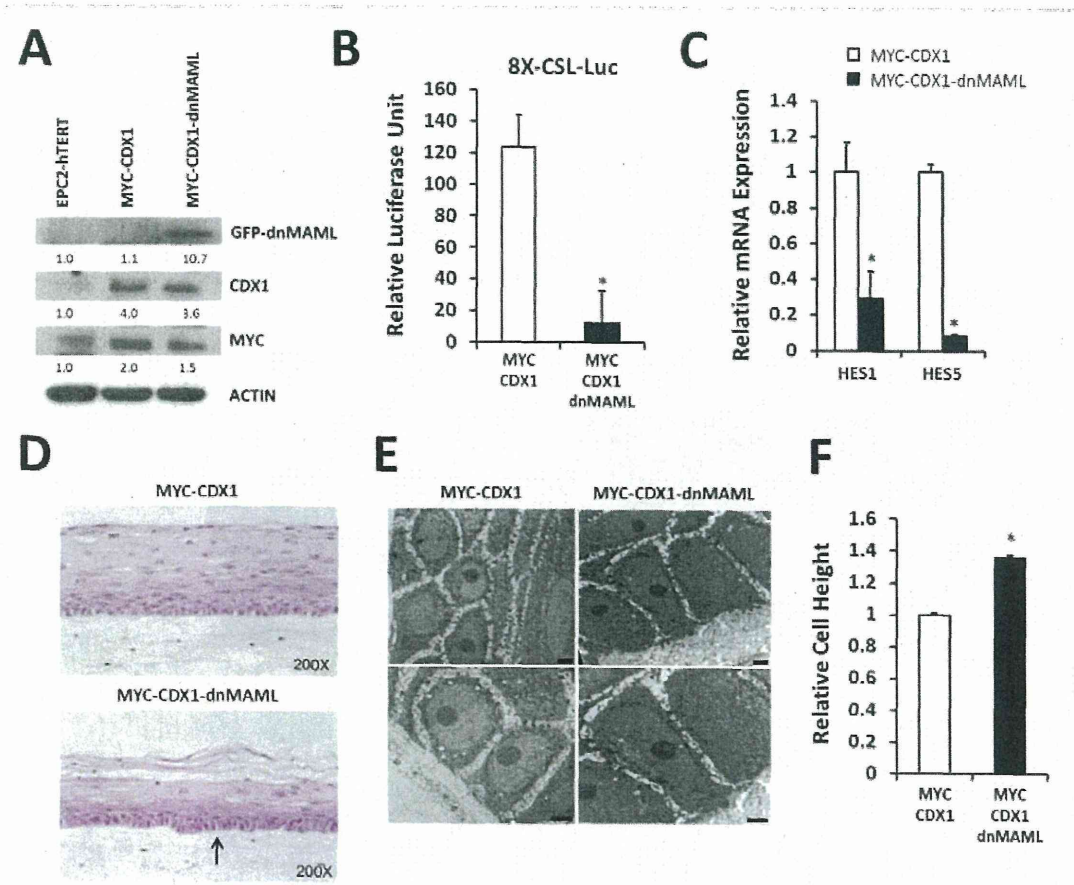
A
EPC2-hTERT
MYC-CDX1
MYC-CDX1-dnMAML
GFP-dnMAML
1.0 1.1 10.7
CDX1
1.0 4.0 3.6
MYC
1.0 2.0 1.5
ACTIN
B
8X-CSL-Luc
Relative Luciferase Unit
160 140 120 100 80 60 40 20 0
MYC CDX1
MYC CDX1 dnMAML
C
MYC-CDX1
MYC-CDX1-dnMAML
Relative mRNA Expression
1.4 1.2 1 0.8 0.6 0.4 0.2 0
HES1
HES5
D
MYC-CDX1
200X
MYC-CDX1-dnMAML
200X
E
MYC-CDX1
MYC-CDX1-dnMAML
F
Relative Cell Height
1.6 1.4 1.2 1 0.8 0.6 0.4 0.2 0
MYC CDX1
MYC CDX1 dnMAML

FIGURE 3

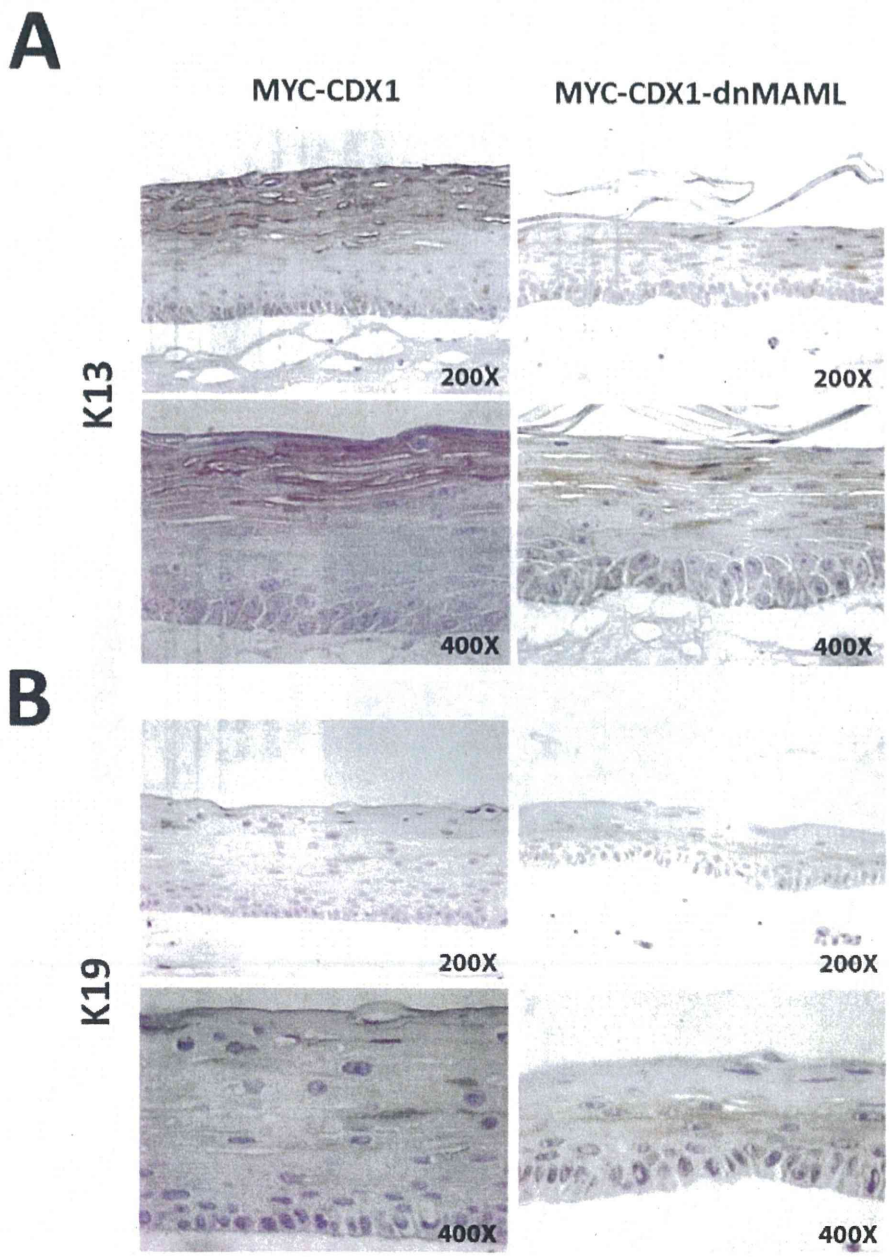
A
MYC-CDX1
MYC-CDX1-dnMAML
K13
200X
200X
400X
400X
B
K19
200X
200X
400X
400X

FIGURE 4

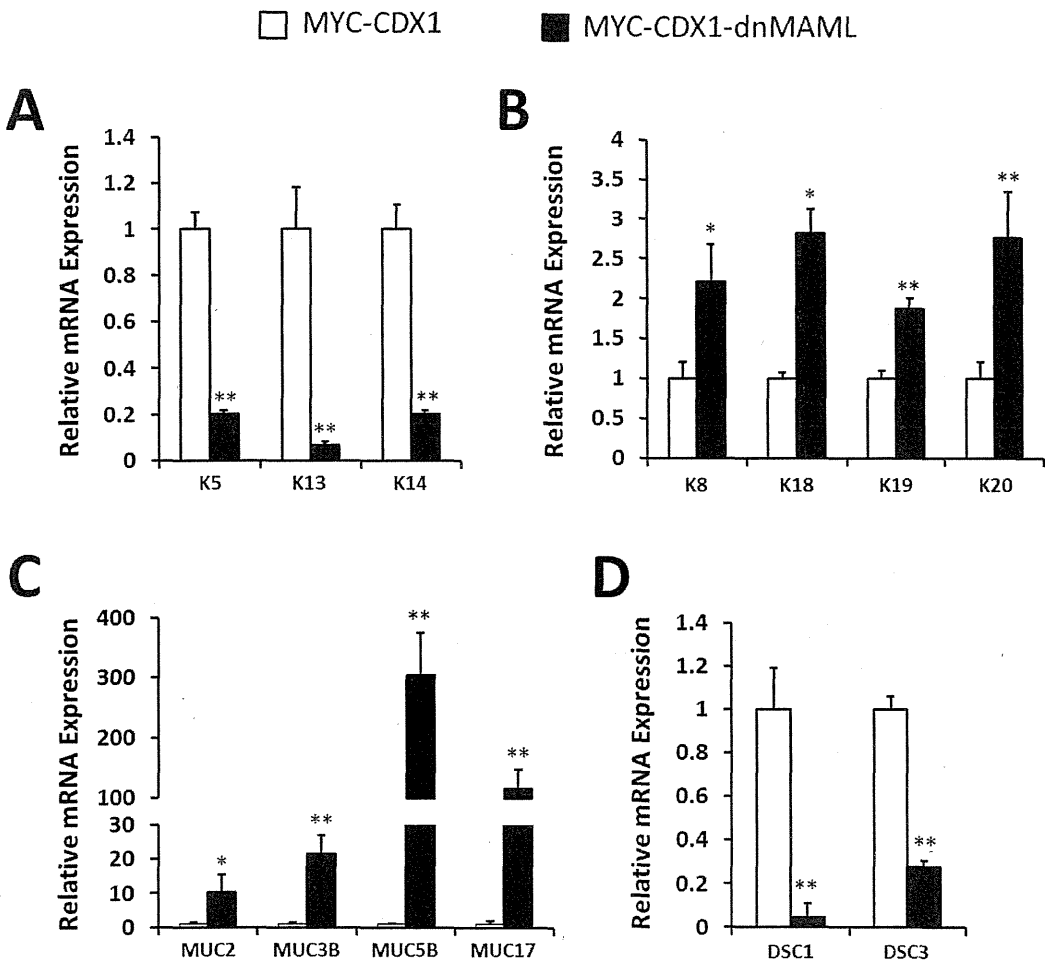
MYC-CDX1
MYC-CDX1-dnMAML
A
Relative mRNA Expression
1.4
1.2
1
0.8
0.6
0.4
0.2
0
K5
K13
K14
B
Relative mRNA Expression
4
3.5
3
2.5
2
1.5
1
0.5
0
K8
K18
K19
K20
C
Relative mRNA Expression
400
300
200
100
30
20
10
0
MUC2
MUC3B
MUC5B
MUC17
D
Relative mRNA Expression
1.4
1.2
1
0.8
0.6
0.4
0.2
0
DSC1
DSC3

FIGURE 5

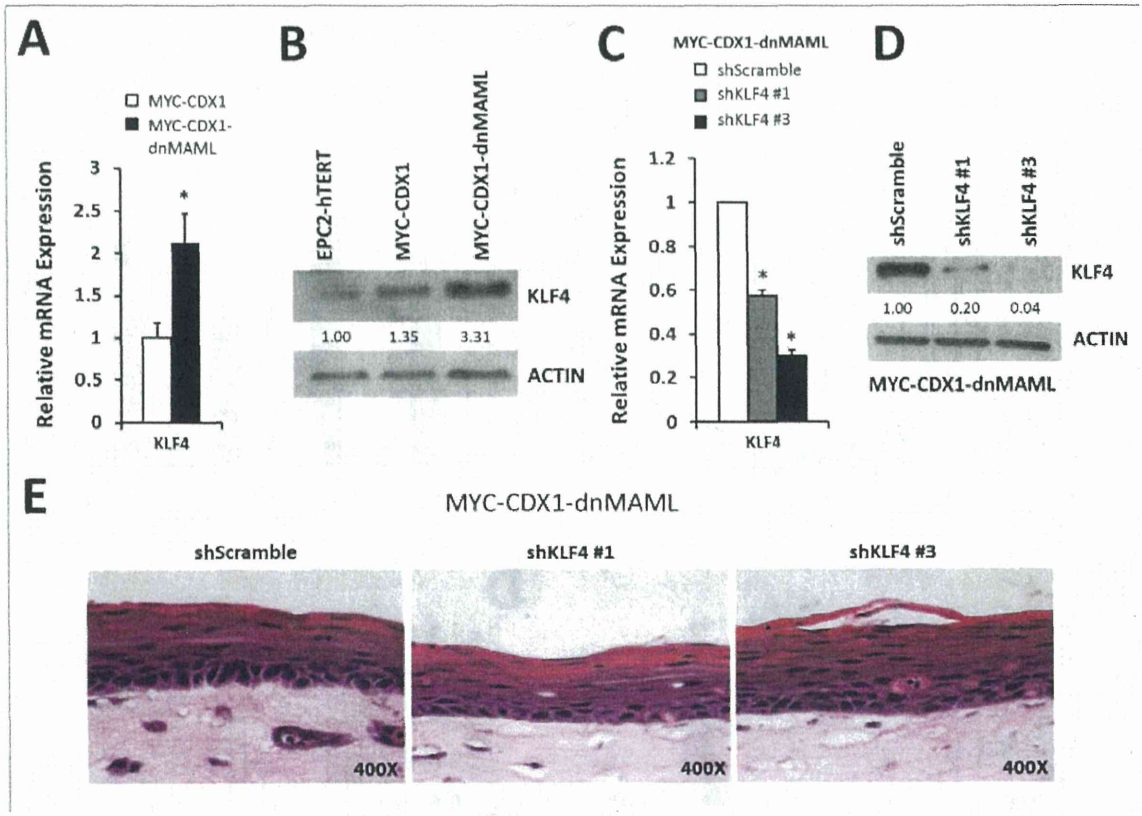
A
MYC-CDX1
MYC-CDX1-dnMAML
Relative mRNA Expression
3
2.5
2
1.5
1
0.5
0
*
KLF4
B
EPC2-hTERT
MYC-CDX1
MYC-CDX1-dnMAML
KLF4
1.00
1.35
3.31
ACTIN
C
MYC-CDX1-dnMAML
shScramble
shKLF4 #1
shKLF4 #3
Relative mRNA Expression
1.2
1
0.8
0.6
0.4
0.2
0
*
*
KLF4
D
shScramble
shKLF4 #1
shKLF4 #3
KLF4
1.00
0.20
0.04
ACTIN
MYC-CDX1-dnMAML
E
MYC-CDX1-dnMAML
shScramble
shKLF4 #1
shKLF4 #3
400X
400X
400X

FIGURE 6

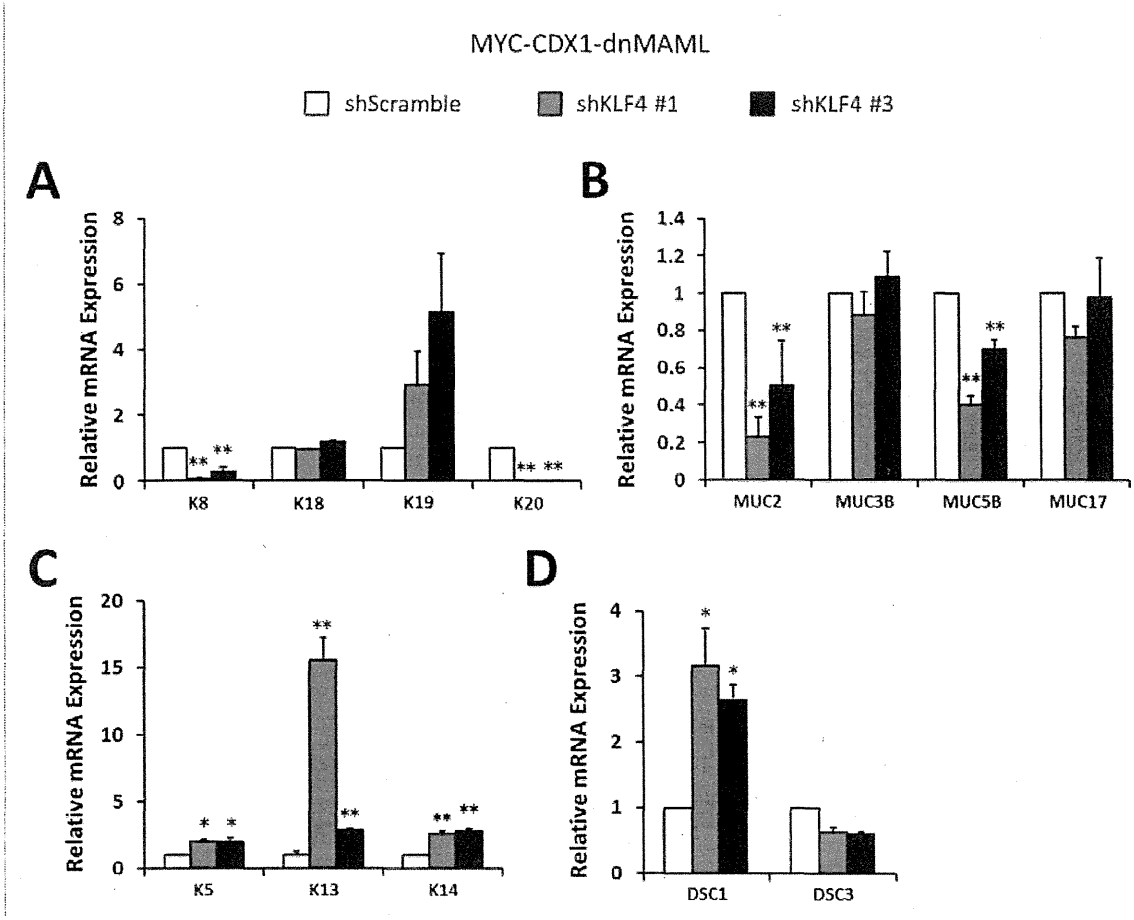
MYC-CDX1-dnMAML
shScramble
shKLF4 #1
shKLF4 #3
A
Relative mRNA Expression
K8
K18
K19
K20
B
Relative mRNA Expression
MUC2
MUC3B
MUC5B
MUC17
C
Relative mRNA Expression
K5
K13
K14
D
Relative mRNA Expression
DSC1
DSC3

FIGURE 7

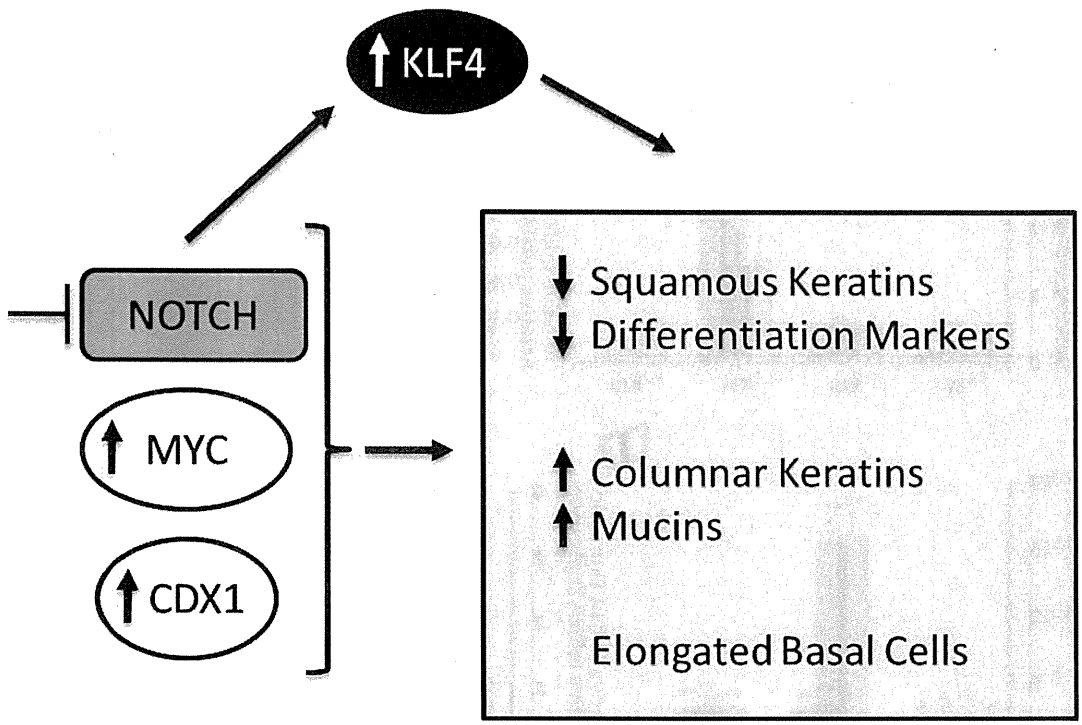
KLF4
NOTCH
MYC
CDX1
Squamous Keratins
Differentiation Markers
Columnar Keratins
Mucins
Elongated Basal Cells

J Gastroenterol
DOI 10.1007/s00535-014-0954-y

The Japanese Society of Gastroenterology

ORIGINAL ARTICLE—LIVER, PANCREAS, AND BILIARY TRACT

CTNNB1 mutational analysis of solid-pseudopapillary neoplasms of the pancreas using endoscopic ultrasound-guided fine-needle aspiration and next-generation deep sequencing

Yoshimasa Kubota · Hiroshi Kawakami · Mitsuteru Natsuizaka · Kazumichi Kawakubo · Katsuji Marukawa · Taiki Kudo · Yoko Abe · Kimitoshi Kubo · Masaki Kuwatani · Yutaka Hatanaka · Tomoko Mitsuhashi · Yoshihiro Matsuno · Naoya Sakamoto

Received: 30 January 2014 / Accepted: 19 March 2014

Abstract
Background Solid-pseudopapillary neoplasm (SPN), a rare neoplasm of the pancreas, frequently harbors mutations in exon 3 of the cadherin-associated protein beta 1 (*CTNNB1*) gene. Here, we analyzed SPN tissue for *CTNNB1* mutations by deep sequencing using next-generation sequencing (NGS).
Methods Tissue samples from 7 SPNs and 31 other pancreatic lesions (16 pancreatic ductal adenocarcinomas (PDAC), 11 pancreatic neuroendocrine tumors (PNET), 1 acinar cell carcinoma, 1 autoimmune pancreatitis lesion, and 2 focal pancreatitis lesions) were analyzed by NGS for mutations in exon 3 of *CTNNB1*.
Results A single-base-pair missense mutations in exon 3 of *CTNNB1* was observed in all 7 SPNs and in 1 of 11 PNET samples. However, mutations were not observed in the tissue samples of any of the 16 PDAC or other four pancreatic disease cases. The variant frequency of *CTNNB1* ranged from 5.4 to 48.8 %.
Conclusions Mutational analysis of *CTNNB1* by NGS is feasible and was achieved using SPN samples obtained by endoscopic ultrasound-guided fine needle aspiration.

Y. Kubota · H. Kawakami (✉) · M. Natsuizaka · K. Kawakubo · T. Kudo · Y. Abe · K. Kubo · M. Kuwatani · N. Sakamoto
Department of Gastroenterology and Hepatology, Hokkaido University Graduate School of Medicine, Kita-15, Nishi-7, Kita-ku, Sapporo 060-8638, Japan
e-mail: hiropon@med.hokudai.ac.jp

K. Marukawa · Y. Hatanaka · T. Mitsuhashi · Y. Matsuno
Department of Surgical Pathology, Hokkaido University Hospital, Sapporo, Japan

Published online: 04 April 2014

Keywords *CTNNB1* · Solid-pseudopapillary neoplasms of the pancreas · Endoscopic ultrasound-guided fine-needle aspiration (EUS-FNA) · Next-generation sequencing

Introduction

Solid-pseudopapillary neoplasm (SPN) of the pancreas is a rare tumor that accounts for 0.2–2.7 % of all pancreatic tumors [1], predominantly seen in young female patients. It was first described by Frantz [2] in 1959. SPN of the pancreas is characterized by low-grade malignant potential, with an incidence of metastasis of 15 %, and tends to have a favorable prognosis with surgical resections, considered the standard of care, with a 5-year overall survival rate of more than 95 % [1, 3, 4].

β-Catenin is a submembranous component of the cadherin-mediated cell adhesion system and acts as a downstream transcriptional activator of Wnt signaling. Under normal conditions, cytoplasmic β-catenin is expressed at a low level. Phosphorylation of both adenomatous polyposis coli (APC) and axin by glycogen synthase kinase-3β (GSK-3β) enhances β-catenin binding to the APC-axin complex and targets the protein for ubiquitination and proteasomal degradation [5]. In the nucleus, β-catenin forms complexes with proteins such as Tcf and Lef-1 [6], and activates the transcription of several oncogenic genes including c-myc and cyclin D1.

Mutations in exon 3 of the β-catenin gene (also called *CTNNB1*) are reported in approximately 83–100 % [7–12] of surgically resected SPN samples. Accordingly, these mutations are considered a unique genetic characteristic of SPNs, differentiating them from other pancreatic tumors.

Direct sequencing is considered the gold standard for mutational analysis. However, it is difficult to detect a

small proportion of mutant genes using this method. Recently, next-generation sequencing (NGS) has enabled the evaluation of multiple genes for genomic alterations in a single tumor, with high accuracy [13]. Less frequent mutations can also be detected if deep sequencing is performed.

Several studies have described the usefulness of EUS-guided fine-needle aspiration (EUS-FNA) for diagnosing SPNs [14–18]. SPNs could be seen as well-demarcated, hypoechoic, solid masses that sometimes coexist with cystic lesions and/or calcification on EUS. Accuracy of preoperative SPN diagnosis by EUS-FNA is reported to be 75–100 % [17, 18]; however, diagnosis by EUS-FNA is sometimes difficult because of interpretative, sampling, and misclassification errors or insufficient material for immunostaining [19]. In addition, EUS-FNA samples sometimes contain tumor cells that are too small to use for sequencing analysis by polymerase chain reaction (PCR)-based direct sequencing.

In the present study, we analyzed *CTNNB1* mutations using EUS-FNA samples and NGS. To the best of our knowledge, this is the first report of *CTNNB1* mutational analysis using EUS-FNA samples and NGS.

Methods

Samples

Thirty-eight samples were tested: 7 SPNs, 16 pancreatic ductal adenocarcinomas (PDAC), 11 pancreatic neuroendocrine tumors (PNET), and 4 other pancreatic lesions. Non-SPN samples were used as controls. Samples were obtained by either EUS-FNA ($n = 35$) or surgery ($n = 3$) at Hokkaido University Hospital, Sapporo, Japan, between December 2008 and June 2013. All participants provided written informed consent, and the ethics committee at Hokkaido University Graduate School of Medicine approved the study.

EUS-FNA procedure

EUS-FNA was performed by a single experienced endoscopist (H.K.) using a curvilinear echoendoscope (GF-UCT240-AL5; Olympus Medical Systems Co., Tokyo, Japan) and 22-gauge needles (Echotip Ultra; Cook Japan, Tokyo, Japan) with the patient under conscious sedation. Briefly, the lesions were visualized by EUS, and the needle was advanced into the lesion through the gastric or duodenal wall. The central stylet was removed, and a syringe was attached to the needle hub to apply negative suction pressure. The needle was then moved back and forth within the lesion at least 10 times and then removed through the scope, before the stylet was re-inserted into the needle. The specimen obtained by aspiration was placed on a slide, air-dried, alcohol-fixed, and used to prepare smears that were stained using the rapid Romanowsky technique for quick interpretation and assessment of sample adequacy (Diff-Quik stain; Kokusai Shiyaku, Kobe, Japan). Diff-Quik staining was performed on all specimens by an experienced cytotechnologist (K.M.). Cytological and histological diagnoses were made for the specimens obtained by EUS-FNA [20, 21].

DNA extraction, PCR, and sequencing analysis of *CTNNB1*

The FNA samples were stored in RNAlater (Life Technologies Corporation, Carlsbad, CA). Genomic DNA and RNA were extracted from samples using an AllPrep® DNA/RNA/Protein mini kit (Qiagen, Inc., Valencia, CA) according to the manufacturer's instructions. Three PNET samples were obtained from surgery. Tumor samples were fixed in 10 % buffered formalin and embedded in paraffin for microdissection of the tumor tissue. Genomic DNA was semi-automatically extracted using a QIAamp® DNA FFPE tissue kit (Qiagen) and QIAcube® (Qiagen) according to the manufacturer's instructions. Total RNA concentration was determined by spectrophotometer (NanoDrop2000/2000c; Thermo Scientific, Tokyo, Japan), and 5 μg total RNA were reverse transcribed using SuperScript® II Reverse Transcriptase (Invitrogen, Carlsbad, CA). Approximately 100 ng of each genomic DNA sample were used for PCR. Genomic DNA was amplified by semi-nested PCR, using the first and second primer pairs (Table 1). Primers for the second PCR contained adaptors and barcodes for further NGS analysis, and the PCR products were bidirectionally read by NGS. These primers were designed to amplify a 228-bp DNA fragment of the entire exon 3 of *CTNNB1*. The thermal cycler (Life Technologies) was programmed as follows: initial denaturation at 94 °C for 7 min and 35 amplification cycles for each PCR. Each amplification cycle comprised denaturation at 94 °C for 15 s, annealing at 58 °C for 15 s, and elongation at 72 °C for 30 s. The last cycle was followed by a final extension at 72 °C for 5 min. The PCR products were verified by agarose gel electrophoresis. The band of the expected size was excised and purified using a QIAquick® Gel Extraction kit (Qiagen).

The concentration and amplicon size of the barcoded libraries were determined by using an Agilent 2100 Bioanalyzer and Agilent DNA 1000 kit (Agilent Technologies, Inc., Santa Clara, CA).

They were pooled and mixed with Ion Spheres™ particles for emulsion PCR using the Ion OneTouch™ System (Life Technologies) with an Ion OneTouch™

Table 1 Primers used in this study

Primers for the first PCR
Forward
5́-CTGATTTGATGGAGTTGGACATGG-3́
Reverse
5́-CAGCTACTTGTTCTTGAGTGAAGG-3́
Primers for the second PCR (library preparation for next-generation sequencing)
Primer pair for forward sequencing
Forward
5́-CCATCTCATCCCTGCGTGTCTCCGACTCAG-barcode-CTGATTTGATGGAGTTGGACATGG-3́
Reverse
5́-CCTCTCTATGGGCAGTCGGTGATCAGCTACTTGTTCTTGAGTGAAGG-3́
Primer pair for reverse sequencing
Forward
5́-CCATCTCATCCCTGCGTGTCTCCGACTCAG-barcode-CAGCTACTTGTTCTTGAGTGAAGG-3́
Reverse
5́-CCTCTCTATGGGCAGTCGGTGATCTGATTTGATGGAGTTGGACATGG-3́

Template kit v2 (Life Technologies) according to the manufacturer's instructions. Samples were subsequently enriched using Ion OneTouch™ ES (Life Technologies). The final concentration of the template for emulsion PCR was 0.4 pM. Sequencing was performed on an Ion PGM™ (Personal Genome Machine) Sequencer by using an Ion 314™ chip (Life Technologies) with an Ion-PGM™ Sequencing 200 kit (Life Technologies) according to the manufacturer's protocol. Obtained sequences were mapped onto the human reference genome hg19, and variants were detected using Ion Torrent Suite v2.2 software (Life Technologies).

The PCR products were also submitted to direct sequencing using ABI Big Dye Terminator v1.1 Cycle Sequencing Kit (Applied Biosystems, Foster City, CA) and the primers used for PCR. Sequencing of each PCR product was performed with an ABI PRISM™ 310 Genetic Analyzer (Applied Biosystems). Each mutation was verified in both sense and antisense directions.

Results

Clinicopathological features

The clinicopathological features of the 38 patients are summarized in Table 2. The patient population comprised 24 women and 14 men, with ages ranging from 13 to 81 years (median 63.5 years). SPNs tended to be located in the pancreatic body and tail rather than in the pancreatic head. Other tumors involved all parts of the pancreas and were evenly distributed. Tumor sizes ranged from 8 to 95 mm at the greatest diameter (median 23 mm).

The types of surgical procedures were as follows: three subtotal stomach-preserving pancreaticoduodenectomies, two duodenum-preserving pancreas head resections, seven distal pancreatectomies (four with splenectomy and one with spleen and left adrenal gland resection), one partial pancreatectomy, and one left nephrectomy with metastatic lymph node tumor resection. Two patients with PDAC had resectable disease, whereas the other cases were unresectable.

The histological features of the specimens with SPN obtained by EUS-FNA are shown in Fig. 1. In most cases, SPN showed typical findings, but in case 7, SPN was not easily distinguished from PNET. Immunohistochemical staining was performed for SPN and PNET samples. Two SPNs showed a few chromogranin A-positive cells, five of seven SPNs showed immunoreactivity against Synaptophysin, and five SPNs showed nuclear staining for β-catenin. All PNET samples were positive for chromogranin A and synaptophysin, and none showed nuclear immunoreactivity against β-catenin.

Genomic DNA and RNA were extracted from FNA samples in 35 patients. For three PNET patients (Case 24, 25 and 26), surgically resected specimens were used to obtain DNA.

Mutations in exon 3 of *CTNNB1* by NGS

All seven SPNs showed a single-base-pair missense mutation in exon 3 of *CTNNB1*. Neither the PDAC nor acinar cell carcinoma cases showed a *CTNNB1* exon 3 mutation. Of the 11 PNETs, a single-base-pair missense mutation was detected in one sample. Variant frequency and coverage ranged from 5.4 to 48.8 % and from 4,490 to

Table 2 Clinicopathological features

Case	Final diagnosis	Sex	Age	Location in pancreas	Tumor size (mm)	Radiological feature	Tumor markers		Procedure for the final diagnosis	Surgical procedure	Results of immunohistochemical staining		
							CEA (ng/mL)	CA19-9 (IU/mL)			CgA	Synaptophysin	β-Catenin
1	SPN	F	33	Pt	64	Solid/cystic	2	0	Surgery	DP	(−)	(+)	Nuclear
2	SPN	F	31	Pb	12	Solid/cystic	1	6	Surgery	Partial pancreatectomy	(−)	(−)	Nuclear
3	SPN	F	17	Ph	23	Solid/cystic	1	<1	Surgery	DpPHR	(−)	(+)	ND
4	SPN	F	36	Pbt	28	Solid/cystic	2	12	Surgery	DP	(−)	(+)	Nuclear
5	SPN	F	27	Pt	48	Solid/cystic	1	<1	Surgery	DP	(+)	(+)	Nuclear
6	SPN	F	13	Ph	63	Solid/cystic	1	9	Surgery	DpPHR	(+)	(+)	Nuclear
7	SPN	F	26	Pb	13	Solid	1	8	EUS-FNA	ND	(−)	(−)	ND
8	PDAC	F	64	Ph	33	Solid	10	3	Surgery	SSPPD	ND	ND	ND
9	PDAC	F	75	Pt	22	Solid	55	220	Surgery	DP	ND	ND	ND
10	PDAC	F	55	Ph	45	Solid	12	693	EUS-FNA	ND	ND	ND	ND
11	PDAC	M	62	Pt	70	Solid	79	>10,000	EUS-FNA	ND	ND	ND	ND
12	PDAC	F	76	Ph	70	Solid/cystic	4	>10,000	EUS-FNA	ND	ND	ND	ND
13	PDAC	M	64	Ph	17	Solid	22	53	EUS-FNA	ND	ND	ND	ND
14	PDAC	F	81	Ph	9	Solid	2	21	EUS-FNA	ND	ND	ND	ND
15	PDAC	F	78	Pt	66	Solid	12	361	EUS-FNA	ND	ND	ND	ND
16	PDAC	F	67	Ph	10	Solid	7	242	EUS-FNA	ND	ND	ND	ND
17	PDAC	M	63	Ph	27	Solid	7	2,320	EUS-FNA	ND	ND	ND	ND
18	PDAC	M	57	Ph	17	Solid	6	30	EUS-FNA	ND	ND	ND	ND
19	PDAC	M	79	Ph	30	Solid	3	871	EUS-FNA	ND	ND	ND	ND
20	PDAC	M	44	Pbt	28	Solid	48	2,880	EUS-FNA	ND	ND	ND	ND
21	PDAC	M	78	Pt	27	Solid	3	229	EUS-FNA	ND	ND	ND	ND
22	PDAC	F	67	Ph	25	Solid	15	246	EUS-FNA	ND	ND	ND	ND
23	PDAC	M	80	Pt	47	Solid	440	>10,000	EUS-FNA	ND	ND	ND	ND
24	PNET	F	58	Pt	23	Solid	2	14	Surgery	DP	(+)	(+)	ND
25	PNET	M	51	Ph	52	Solid/cystic	2	31	Surgery	SSPPD	(+)	(+)	ND
26[a]	PNET	F	76	Lymph node	18	Solid	3	11	Surgery	Left nephrectomy	(+)	(+)	ND
27[b]	PNET	M	72	Pt	20	Solid	5	14	Surgery	DP	(+)	(+)	ND
28	PNET	F	58	Pb	18	Solid	2	14	Surgery	DP	(+)	(+)	ND
29	PNET	F	78	Ph	16	Solid	2	<1	Surgery	SSPPD	(+)	(+)	ND
30	PNET	M	79	Pb	9	Solid	3	8	EUS-FNA	ND	(+)	(+)	Membrane
31	PNET	F	69	Pt	8	Solid	3	5	EUS-FNA	ND	(+)	(+)	ND
32	PNET	F	77	Ph	17	Solid	2	47	EUS-FNA	ND	(+)	(+)	ND
33	PNET	F	45	Ph	17	Solid/cystic	3	26	EUS-FNA	ND	(+)	(+)	ND

Table 2 continued

Case	Final diagnosis	Sex	Age	Location in pancreas	Tumor size (mm)	Radiological feature	Tumor markers		Procedure for the final diagnosis	Surgical procedure	Results of immunohistochemical staining		
							CEA (ng/mL)	CA19-9 (IU/mL)			CgA	Synaptophysin	β-Catenin
34	PNET	F	62	Ph	10	Solid/cystic	6	40	EUS-FNA	ND	(+)	(+)	ND
35	Acinar cell carcinoma	M	46	Pbt	95	Solid/cystic	4	19	EUS-FNA	ND	(+)	(−)	ND
36	AIP	M	72	Pt	28	Solid	8	22	EUS-FNA	ND	ND	ND	ND
37	Focal pancreatitis	F	42	Pt	20	Solid/cystic	1	6	EUS-FNA	ND	ND	ND	ND
38	Focal pancreatitis	M	64	Ph	22	Solid	4	<1	EUS-FNA	ND	ND	ND	ND

SPN solid-pseudopapillary neoplasm, *PDAC* pancreatic ductal adenocarcinoma, *PNET* pancreatic neuroendocrine tumor, *AIP* autoimmune pancreatitis, *M* male, *F* female, *Ph* pancreatic head, *Pb* pancreatic body, *Pt* pancreatic tail, *CEA* carcinoembryonic antigen, *CA19-9* carbohydrate antigen 19-9, *EUS-FNA* endoscopic ultrasound-guided fine-needle aspiration, *DP* distal pancreatectomy, *DpPHR* duodenum-preserving pancreas head resection, *SSPPD* subtotal stomach-preserving pancreaticoduodenectomy, *CgA* chromogranin A, *ND* not done

[a] The patient of case 26 developed a metastatic lymph node tumor 5 years after the initial surgery for PNET. Secondary surgery was a left nephrectomy with metastatic lymph node tumor resection

[b] The patient of case 27 had mixed ductal-neuroendocrine carcinoma and two synchronous PNETs

203,919, respectively. For the sample with a variant frequency of 5.39, the read depth was 15,199. The involved codons were as follows: codon 32 (three cases), codon 37 (two cases), and codon 41 (three cases). The results of the analysis are shown in Table 3. For the control samples, the average base coverage depth ranged from 113 to 8,027 (median 7,312).

Mutations in exon 3 of *CTNNB1* by direct sequencing

Direct sequencing was performed using samples that had mutations detected by NGS. One SPN case with mutation was not able to perform direct sequencing due to an insufficient amount of the sample. Only one of the seven cases could detect mutation by direct sequencing, as shown also in Table 3.

Discussion

Mutations in exon 3 of *CTNNB1* have been reported in various tumors, including those of the colon [22], prostate [23], endometrium [24], and liver [25].

In SPN, cytoplasmic/nuclear immunoreactivity for β-catenin was detected during the systemic immunohistochemical study of pediatric tumors [7]. After the first report by Tanaka et al. [7], mutations in exon 3 of *CTNNB1* have been reported in 83–100 % [7–12] of SPNs. Previous studies used microdissected tumor tissue from formalin-fixed, paraffin-embedded blocks obtained by surgery to extract genomic DNA. Single-base-pair missense mutations in codons 32, 33, 34, 37, and 41, and 12-base-pair deletion corresponding to codons 28–32 have been documented.

Serine 33 and 37 as well as threonine 41 are the sites for GSK-3 β phosphorylation [26]. Codons 32 and 34 serve as crucial elements of the DSGΦXS motif to create a recognition site for β-TrCP and subsequent ubiquitin-mediated proteasomal degradation [27, 28]. Both mechanisms lead to the abnormal stabilization of β-catenin and its resultant aberrant nuclear expression in SPNs.

In the present study, eight cases showed *CTNNB1* mutations. Mutations were detected in codons 32, 37, and 41, consistent with the findings of previous reports [7–12]. To the best of our knowledge, this is the first report of mutational analysis for *CTNNB1* using EUS-FNA samples and NGS. Of the eight cases, seven were of SPN and one was of PNET. That PNET was diagnosed by the typical radiologic finding (a hypervascular round mass that was best visualized in the arterial contrast enhancement phase on computed tomography) and immunohistochemical staining (positive chromogranin A and synaptophysin immunostaining, negative CD56 staining, and no nuclear

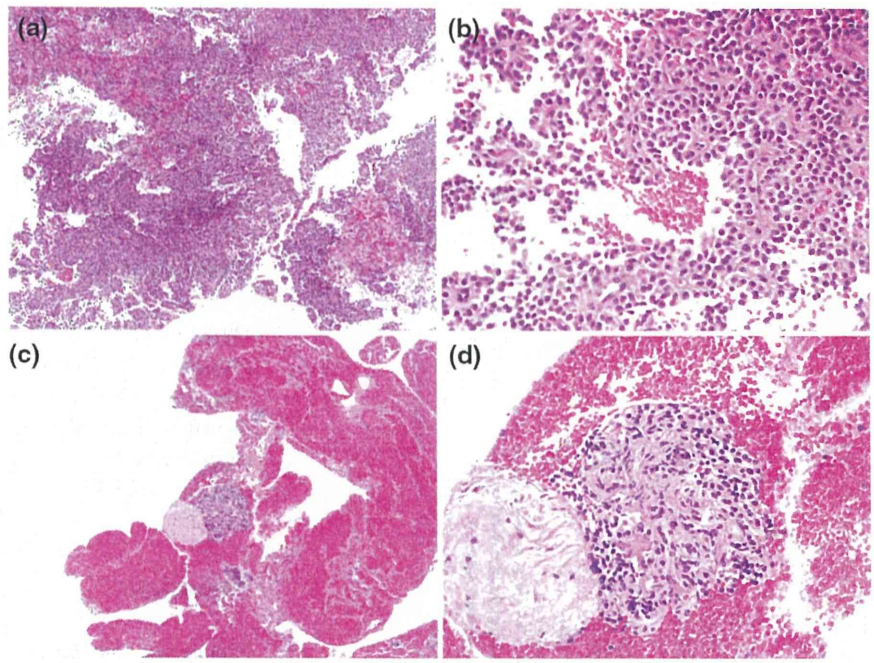

Fig. 1 Histological features of solid-pseudopapillary neoplasm specimens obtained by endoscopic ultrasonography-guided fine-needle aspiration. **a**, **b** Typical specimen (case 4). Small and uniform neoplastic cells have either eosinophilic or clear vacuolated cytoplasm. These loosely cohesive cells surround the delicate vessels and form pseudopapillae. **c**, **d** Atypical specimen (case 7). The specimen contains a small number of neoplastic cells in the fibrous stroma that do not form apparent pseudopapillae. The small and uniform neoplastic cells have eosinophilic cytoplasm and show a plasmacytoid appearance. These clusters are difficult to distinguish from those of neuroendocrine tumors

Table 3 Mutations in *CTTNB1*

Case	Template	Mutated codon	Nucleotide	AA substitution	Var. freq (%)	Coverage	Ref cov.	Var cov.	Direct seq
1	RNA	37	N378 C/A	Ser37Tyr	23.81	19,047	14,495	4,535	Undetectable
2	RNA	32	N363 A/G	Asp32Gly	5.39	16,072	15,199	866	Undetectable
3	RNA	32	N362 G/C	Asp32His	48.77	25,740	13,161	12,554	Undetectable
4	gDNA	41	N390 C/T	Thr41Ile	31.07	4,490	3,093	1,395	Undetectable
5	gDNA	37	N378 C/T	Ser37Phe	26.48	115,799	84,609	30,665	Detectable
6	gDNA	41	N362 G/A	Asp32Asn	21.50	203,919	43,842	160,077	Undetectable
7	RNA	41	N390 C/T	Thr41Ile	29.68	35,808	25,167	10,629	NA

AA amino acid, *Var Freq* variant frequency, *Ref Cov* reference coverage, *Var Cov* variantcoverage, *Direct seq* direct sequencing, *gDNA* genomic DNA, *Ser* serine, *Tyr* tyrosine,*Asp* asparatic acid, *Gly* glycine, *His* histidine, *Thr* threonine, *Ile* isoleucine, *Phe*phenylalanine, *Asn* asparagine, *NA* not available

β-catenin accumulation) of an EUS-FNA sample. The patient did not undergo surgery because of the small size (9.6 × 5.4 mm) and low-grade malignant potential of the lesion, which was diagnosed on the basis of EUS-FNA specimen analysis (Ki-67 index, 1–2 %).

Several assays can be performed to detect genetic mutations, such as hematoxylin and eosin and immunohistochemical staining, fluorescence in-situ hybridization, polymerase chain reaction, and direct sequencing. Although direct sequencing is considered the gold standard, it lacks the ability to detect small proportions of mutant genes and technical experience is essential for accurate result interpretation. In one study, mutant DNA had to account for at least 30 % of wild-type DNA for the detection of mutations by direct sequencing [29]. In our study, mutations caught by NGS could be detected in only one of seven samples by direct sequencing. Our result showed the superiority of NGS in detecting mutations over direct sequencing, as indicated in previous reports. This result suggests the usefulness of FNA specimens for genetic analyses when combined with NGS, since EUS-FNA specimens are usually mixed with blood or tissue in the needle tract.

To date, *CTNNB1* mutations have not been reported in PNET. Gerdes et al. [30] previously performed *CTNNB1* mutational analysis on 78 PDAC, 33 PNET, and 14 pancreatic cancer cell lines and found no mutations in exon 3 of *CTNNB1*. Similarly, Liu et al. [10] found no mutations in exon 3 of *CTNNB1* in 14 PNET samples. Exome sequence analysis of approximately 18,000 protein-coding

genes of 10 PNET samples was carried out by Jiao et al. [31] to explore the genetic basis of the disease. They reported novel *DAXX* and *ATRX* mutations, but mutations in *CTNNB1* were not detected. With regard to neuroendocrine tumors in other organs, Kim et al. [32] detected a single-base-pair mutation in one of two thymus neuroendocrine tumors, which resulted in a replacement of isoleucine by serine at codon 35. Another mutation was seen in a cell line of neuroendocrine tumor of midgut (terminal ileum) origin [33]. To explore whether *CTNNB1* mutations occur in PNET, we enrolled two more cases of PNET that were diagnosed by surgery, but did not detect any mutations. Further analysis should be performed to determine if *CTNNB1* mutations occur in PNET.

One of the most important differential diagnoses of SPN is PNET [16, 34]. Histologically, most SPNs show a solidmonomorphous growth in the peripheral parts of the lesion. In the center, tumor cells form pseudopapillary structures [35]. PNETs are morphologically very similar to SPNs. Immunostaining is useful in differentiating SPNs from PNETs. SPNs specifically express vimentin and CD10 [8, 36] and usually show focal immunoreactivity against synaptophysin, but not for chromogranin A. On the other hand, PNETs usually show diffuse staining for synaptophysin. Strong staining for chromogranin A is observed in differentiated neuroendocrine tumors, NETs, but negative or very mild staining is found in poorly differentiated lesions [37, 38]. β-Catenin localization is also quite different between these two tumor types. SPNs show cytoplasmic and nuclear staining [3, 7], but PNETs show membranous staining. Accurate diagnosis of SPNs is sometimes difficult with EUS-FNA because of interpretative, sampling, and misclassification errors or insufficient material for immunostaining [19]. In the present study, 1 case of SPN could not be diagnosed pathologically on the basis of EUS-FNA samples. However, the *CTNNB1* mutation was detected by NGS, and the patient was diagnosed as having SPN and was scheduled for surgery at the time of reporting.

The current study was limited by two points. First, not all of the mutational analyses were performed prior to the final diagnosis by either EUS-FNA or surgery. Second, being a rare tumor, the sample size was rather small.

Conclusions

Analysis of exon 3 mutations in *CTNNB1* by NGS is feasible using EUS-FNA samples. All SPN cases showed *CTNNB1* mutations. Further exploration of mutational analyses including *CTNNB1* in neuroendocrine tumors is required to determine the genetic alterations of PNET.

Conflict of interest The authors declare that they have no conflict of interest.

References

1. Papavramidis T, Papavramidis S. Solid pseudopapillary tumors of the pancreas: review of 718 patients reported in English literature. J Am Coll Surg. 2005;200:965–72.
2. Frantz VK. Tumors of the pancreas. Atlas of tumor pathology, 1st series. Washington DC: Armed Forces Institute of Pathology; 1959.
3. Klimstra DS, Wenig BM, Heffess CS. Solid-pseudopapillary tumor of the pancreas: a typically cystic carcinoma of low malignant potential. Semin Diagn Pathol. 2000;17:66–80.
4. Yu PF, Hu ZH, Wang XB, et al. Solid pseudopapillary tumor of the pancreas: a review of 553 cases in Chinese literature. World J Gastroenterol. 2010;16:1209–14.
5. Behrens J, Jerchow BA, Würtele M, et al. Functional interaction of an axin homolog, conductin, with beta-catenin, APC, and GSK3beta. Science. 1998;280:596–9.
6. Aoki M, Hecht A, Kruse U, et al. Nuclear endpoint of Wnt signaling: neoplastic transformation induced by transactivating lymphoid-enhancing factor 1. Proc Natl Acad Sci USA. 1999;96:139–44.
7. Tanaka Y, Kato K, Notohara K, et al. Frequent ß-catenin mutation and cytoplasmic/nuclear accumulation in pancreatic solid-pseudopapillary neoplasm. Cancer Res. 2001;61:8401–4.
8. Abraham SC, Klimstra DS, Wilentz RE, et al. Solid-pseudopapillary tumors of the pancreas are genetically distinct from pancreatic ductal adenocarcinomas and almost always harbor beta-catenin mutations. Am J Pathol. 2002;160:1361–9.
9. Takahashi Y, Hiraoka N, Onozato K, et al. Solid-pseudopapillary neoplasms of the pancreas in men and women: do they differ? Virchows Arch. 2006;448:561–9.
10. Liu BA, Li ZM, Su ZS, et al. Pathological differential diagnosis of solid-pseudopapillary neoplasm and endocrine tumors of the pancreas. World J Gastroenterol. 2010;16:1025–30.
11. Wu J, Jiao Y, Dal Molin M, et al. Whole-exome sequencing of neoplastic cysts of the pancreas reveals recurrent mutations in components of ubiquitin-dependent pathways. Proc Natl Acad Sci USA. 2011;108:21188–93.
12. Huang SC, Ng KF, Yeh TS, et al. Clinicopathological analysis of beta-catenin and axin-1 in solid pseudopapillary neoplasms of the pancreas. Ann Surg Oncol. 2011;19(Suppl 3):S438–46.
13. Ross JS, Ali SM, Wang K, et al. Comprehensive genomic profiling of epithelial ovarian cancer by next generation sequencing-based diagnostic assay reveals new routes to targeted therapies. Gynecol Oncol. 2013;130:554–9.
14. Nadler EP, Novikov A, Landzberg BR, et al. The use of endoscopic ultrasound in the diagnosis of solid pseudopapillary tumor of the pancreas in children. J Pediatr Surg. 2002;37:1370–3.
15. Master SS, Savides T. Diagnosis of solid pseudopapillary neoplasm of the pancreas by EUS-guided FNA. Gastrointest Endosc. 2003;57:965–9.
16. Bardales RH, Centeno B, Mallery JS, et al. Endoscopic ultrasound-guided fine-needle aspiration cytology diagnosis of solid pseudopapillary tumor of the pancreas: a rare neoplasm of elusive origin but characteristic cytomorphologic features. Am J Clin Pathol. 2004;121:654–62.
17. Jani N, Dewitt J, Eloubeidi M, et al. Endoscopic ultrasound-guided fine-needle aspiration for diagnosis of solid pseudopapillary tumors of pancreas: a multicenter experience. Endoscopy. 2008;40:200–3.